Nanoscale

PAPER

View Article Online
View Journal | View Issue

Cite this: *Nanoscale*, 2025, **17**, 5181

Encapsulated ruthenium sites in reaction microenvironment-regulated UiO-66 for stable acetylene hydrochlorination†

Digao Chai,[a] Qidi Liu,[a] Yunsheng Dai,[b] Yongsheng Xu, *[a] Yu Zi,[a] Shuo Yang,[a] Yanzhao Dong,[a] Dongyang Xie,[a] Jinli Zhang [a,c] and Haiyang Zhang *[a]

Received 29th October 2024,
Accepted 17th January 2025

DOI: 10.1039/d4nr04506h

rsc.li/nanoscale

Ruthenium (Ru)-based catalysts have been recognized as potential substitutes for mercury in the hydrochlorination of acetylene due to their high initial activity and low cost. However, rapid deactivation limits their industrial application and the agglomeration of active sites is considered as one of the main reasons for deactivation. To overcome this challenge, in this work, we introduced a thermally stable metal–organic framework to encapsulate Ru sites into regular channels successfully, thus enhancing the dispersion of Ru sites. To decrease the diffusion resistance caused by the channels, we partly substituted –H groups with –OH groups in the channels to change the reaction microenvironment. After characterization and simulation, we demonstrated that both the encapsulation strategy and channel regulation were beneficial for increasing the adsorption of reactants, thus obtaining 92.27% conversion of acetylene with a deactivation rate below 0.02% h^{-1} even when the gas hourly space velocity was at a high level (540 h^{-1}). This work provides a new insight into inhibition of the deactivation of Ru-based catalysts in acetylene hydrochlorination *via* introducing skeleton materials with regular channels.

[a]*School of Chemistry and Chemical Engineering/State Key Laboratory Incubation Base for Green Processing of Chemical Engineering, Shihezi University, Shihezi 832000, P. R. China. E-mail: 2016207134@tju.edu.cn, zhy198722@163.com; Fax: +86-993-2057210; Tel: +86-993-2057006*

[b]*Yunnan Precious Metals Lab Co., Ltd, Kunming 650106, P. R. China*

[c]*School of Chemical Engineering and Technology, Tianjin University, Tianjin 300354, P. R. China*

†Electronic supplementary information (ESI) available. See DOI: **https://doi.org/10.1039/d4nr04506h**

1. Introduction

As the third most versatile resin synthetic material, polyvinyl chloride (PVC) has an extremely wide range of applications and high demand in daily life.[1–3] The acetylene hydrochlorination process is a key industrial unit for the production of the PVC monomer. In industry, $HgCl_2$ is used as a commercial product and a catalyst in the hydrochlorination of acetylene.

Yongsheng Xu

Yongsheng Xu completed his PhD at the age of 29 from Tianjin University and is now an associate professor at Shihezi University. He mainly focuses on catalyst design for acetylene hydrochlorination and Fenton-like reactions. He has published more than 20 papers in reputed journals.

Haiyang Zhang

Haiyang Zhang completed his PhD at the age of 28 from Tianjin University and then a visiting scholar research project at Cardiff University. He is a professor at Shihezi University, a comprehensive research university in China. He is mainly engaged in the research and development of mercury-free catalysts for acetylene hydrochlorination, the design and synthesis of high-performance metal nanocatalysts and other industrial catalysis research, and he has published more than 60 papers in reputed journals.

However, mercury is highly toxic and leakage during production can cause harm to humans and the surrounding environment. With the signing of "The Minamata Convention on Mercury", the substitution of mercury-based catalysts is an inevitable trend. Therefore, it is urgent to develop a green and efficient mercury-free catalyst for the production of the PVC monomer. In the past decades of research, catalysts loaded with Au sites have been found to be extremely active and selective in acetylene hydrochlorination reactions. Thus, gold-based catalysts are regarded as the most likely green alternatives to replace $HgCl_2$. With more research on gold-based catalysts, it has been found that gold-based catalysts are easily deactivated.[4–9] Au^{3+} with catalytically active components is easily reduced to Au^0, thus decreasing the catalytic activity. More importantly, the high price of Au (more than $2700 per ounce) is not favorable for the advancement of industrialization. Therefore, researchers have shifted their focus to other cheap metals to develop another efficient and low-cost catalytic system. As early as 1988, Hutchings *et al.* found that ruthenium chloride catalysts had a high initial activity by comparing the activity of various metal chlorides.[10] Meanwhile, due to the low cost (nearly $470 per ounce), Ru-based catalysts have been gradually recognized as a mercury-free candidate for the hydrochlorination of acetylene. After analyzing the mechanism, it was found that Ru-based catalysts had a high activation capacity for hydrogen chloride, thus exhibiting high initial activity.[11–14]

However, it has been noted that when Ru-based catalysts were applied in this catalytic system, the relative deactivation rate was high.[15–27] That is, the Ru-based catalyst suffers from severe deactivation. Due to the irregular pore structure of commercial activated carbon, it is difficult to anchor Ru species to obtain high dispersion. Therefore, the Ru sites are easy to agglomerate during the reaction process, thus decreasing the catalytic activity. In order to solve this challenge, researchers have made a series of strategies to modify Ru sites or the support. Hou *et al.*[28] doped nitrogen sites into activated carbon *via* pyrolyzing 2-melamine at high temperature, and the N-dopants formed on the surface of activated carbon can increase the dispersion of Ru sites. Wang *et al.*[20] designed a Ru–N coordination structure by introducing ligands to obtain a single-atom dispersion, thus exhibiting excellent stability. Although these strategies both enhance the catalytic activity after optimizing the dispersion of Ru, there are still some challenges to overcome. The modification of the support is usually performed at high treatment temperatures, while the organic ligands coordinating with Ru species are also unstable during the reaction. Considering the regular and adjustable pore channels of metal–organic frameworks (MOFs),[29–32] it has great advantages in limiting the agglomeration of active sites through encapsulating active sites into the channels of the MOF. Xu *et al.*[33] encapsulated Ru nanoparticles in a UiO-66 skeleton to maintain the high dispersion of Ru nanoparticles and the obtained catalyst showed a high conversion rate for CO_2 methanation. However, due to the pore size being less than 5 nm, the diffusion resistance must increase in the continuous reaction system when the MOF is introduced into the catalyst. Besides, for acetylene hydrochlorination, the thermostability of the MOF must be considered.

Based on the challenges of Ru-based catalysts in acetylene hydrochlorination and the advantages of MOF materials, in this work, we selected a thermostable MOF named UiO-66 and then tried to encapsulate the Ru sites into the channels to enhance and stabilize the dispersion of Ru sites before and after reaction. Also, considering the diffusion resistance from the channels, we employed two organic linkers containing –H groups and –OH groups in the preparation of the MOFs to modify the reaction microenvironment around the Ru sites. Then, the obtained catalysts were evaluated in a fixed-bed reactor to compare and analyze the catalytic performance. Combined with the characterization of the fresh and used catalysts and the relative density functional theory (DFT) simulation, the reaction mechanism was also investigated. This work provides a new insight into inhibition of Ru-based catalyst deactivation *via* skeleton materials with regular channels.

2. Experimental and theoretical method

2.1 Materials

Activated carbon (simplified as AC, 40–60 mesh) was purchased from Fujian Sensen Activated Carbon Industry Science and Technology Company. $RuCl_3{\cdot}3H_2O$ (99%), terephthalic acid, 2-hydroxyterephthalic acid, *N*,*N*-dimethylformamide (DMF), and zirconium(IV) chloride (purity 99.8%) were all purchased from Shanghai Adamas Company. The experimental gases including HCl, C_2H_2, helium, and nitrogen (99.99%) were purchased from Shihezi Hongsheng Standard Gases Ltd. All the materials and reagents were used without further purification.

2.2 Preparation of the catalyst

Zr-based MOF. 417 mg of $ZrCl_4$ was weighed and dissolved in 20 mL of DMF : HCl (1 mol L^{-1}) (5 : 1, v/v) solution. After stirring for 20 min, 0.3828 mg of terephthalic acid and 33 mL of DMF solution were added and stirred for another 20 min. The resulting solution was transferred to a 100 mL hydrothermal reactor, and the hydrothermal kettle was placed in an oven at 120 °C for continuous heating for 24 h. Afterwards, the solution was washed repeatedly with DMF solvent and filtered. Finally, the obtained substance was dried in a blast oven at 120 °C for 24 h to obtain UiO-66 crystals. UiO-66-OH was synthesized as above, except that terephthalic acid was replaced with 0.419 mg of 2-hydroxyterephthalic acid.

Baseline catalyst. 0.182 g of $RuCl_3{\cdot}3H_2O$ was dissolved in 35 mL of anhydrous ethanol and stirred continuously for 20 min. Then, 6 g of AC was added to the above solution and stirred for 12 h. Immediately, the above mixture was placed in a water bath at 70 °C for 12 h. Finally, it was placed in a vacuum drying oven at 110 °C and dried for 24 h. The obtained baseline catalyst was denoted as Ru/AC.

Ru-based catalysts with the MOF. The precursor $RuCl_3$ was first dissolved in deionized water. Then, 0.4 g of UiO-66 was added to the mixture and agitated for 2 h. After that, 3 g of AC was added under stirring and the mixture was kept for 4 h. Subsequently, the sample was incubated at 70 °C for 12 h and desiccated at 120 °C for 12 h to obtain the final catalyst, denoted as Ru@UiO-66/AC. The catalyst Ru@UiO-66-OH/AC was prepared as above.

2.3 Catalyst characterization

Transmission electron microscopy (TEM) was conducted using an FEI Tecnai F20. The samples were dispersed in ethanol and supported on carbon-film-coated 200 copper grids before TEM characterization. X-ray photoelectron spectra (XPS) were recorded on a Thermo ESCALAB 250XI system to determine the valence states of different Ru species on the catalysts. The binding energy was calibrated with respect to the C 1s (284.80 eV). Nitrogen adsorption–desorption isotherms were obtained at 77 K using a Macklin ASAP 2460C surface area and porosity analyzer. Fourier transform infrared spectrometry (FTIR) of the catalysts was performed using a Bruker Vertex70 FT-IR spectrophotometer with a DTGS detector. Temperature-programmed desorption (TPD) experiments were conducted using a Quantachrome ChemBET PULSAR TPR/TPD to investigate the adsorption capacity of the catalysts for reactants and products. The sample loading mass was 120 mg. The sample was first pre-treated under C_2H_2 and HCl atmospheres, respectively, for 4 h at the reaction temperature (180 °C), and then pure helium was passed through the samples for 10 min. After that, the samples were heated from 35 °C to 850 °C at a heating rate of 10 °C min^{-1}. The flow gas was helium with a flow rate of 100 mL min^{-1}. Thermogravimetric analysis (TGA) was carried out using a Netzsch STA 449 F5 under a nitrogen atmosphere at a flow rate of 100 mL min^{-1} with a heating rate of 10 °C min^{-1}. Inductively coupled plasma emission spectrometry (ICP-OES) was used to measure the content of Ru in the catalysts with an Agilent ICP-OES730.

2.4 Catalyst evaluation

Catalyst tests were carried out in a fixed-bed microreactor (i.d. of 10 mm) for acetylene hydrochlorination. The volume of the catalyst was fixed at 3 mL. Before the reaction, nitrogen was used to remove water and air and HCl was passed through the reactor to activate the catalyst at a flow rate of 30 mL min^{-1} and a temperature of 180 °C for 30 min. Then, the reactants containing C_2H_2 and HCl were fed through the filter and the reaction temperature maintained at 180 °C. The effluent from the reactor was passed into NaOH solution, followed by analysis using a GC-2014C gas chromatograph.

The acetylene conversion (X_A), the selectivity to VCM (S_{VC}) and the deactivation rate (K_d) were calculated using the following equations:

$$X_A = (\phi_{A_0} - \phi_A)/\phi_{A_0} \times 100\% \quad (1)$$

$$S_{VC} = \phi_{VC}(1 - \phi_A) \times 100\% \quad (2)$$

$$K_d = (X_{A_{max}} - X_{A_{min}})/T \times 100\% \quad (3)$$

where ϕ_{A_0} is defined as the volume percentage of C_2H_2 in the reaction gas; ϕ_A is defined as the volume percentage of remaining C_2H_2 in the product gas; ϕ_{VC} is the volume percentage of VCM in the product: $X_{A_{max}}$ is the highest conversion rate; $X_{A_{min}}$ is the lowest conversion rate; and T is the reaction time.

2.5 Calculation details

The density functional theory (DFT) calculations were carried out using Materials Studio. The structural optimization was performed using the Dmol3 module in Materials Studio, and the Becke–Lee–Yang–Parr (BLYP) functional within generalized gradient approximation (GGA) was used to process the exchange–correlation,[34] which was utilized to describe the expansion of the electronic eigenfunctions. All atoms were fully relaxed until the force, displacement, and energy were less than 0.002 Ha $Å^{-1}$, 0.005 Å, and 10^{-5} Ha, respectively.[35] The charge density preprocessing option was enabled and the maximum value of Subspace Iterative Inverse (DIIS) was set to 6 to significantly improve self-consistent field convergence.

The adsorption energy and formation energy (E) of a complex formed between two molecules, A and B, can be calculated using the following equation:

$$E = E_{complex} - (E_A + E_B) \quad (4)$$

where $E_{complex}$ is the total energy of the molecular complex of A and B, E_A is the energy of component A, and E_B is the energy of component B.

3. Results and discussion

3.1 Characterization of catalysts

To inhibit the agglomeration of Ru sites, the Zr-based MOFs were prepared *via* a traditional hydrothermal method and then introduced into the Ru-based catalyst system. Considering the diffusion resistance of reactants from the channels of the MOF, we selected two organic linkers including terephthalic acid (without –OH in the channels, the relative MOF is marked as UiO-66) and 2-hydroxyterephthalic acid (with abundant –OH in the channels, the relative MOF is marked as UiO-66-OH) to change the microenvironment of the channels. The structures of pristine UiO-66 and UiO-66-OH were confirmed by X-ray diffraction (XRD). The XRD patterns display the same diffraction peaks at 2θ values of 7.3° and 8.5° (Fig. 1a), agreeing well with the (111) and (200) planes of simulated UiO-66.[36] No diffraction peaks of other impurities were present in the pattern of UiO-66-OH, indicating the pure phase of UiO-66. To further confirm the formation of the UiO-66 structure, nitrogen adsorption–desorption isotherms were obtained. It is shown that UiO-66 and UiO-66-OH have high specific surface areas, whose values reach 749 and 794 m^2 g^{-1}, respectively (Fig. 1b). Then we tried to encapsulate the Ru sites into the

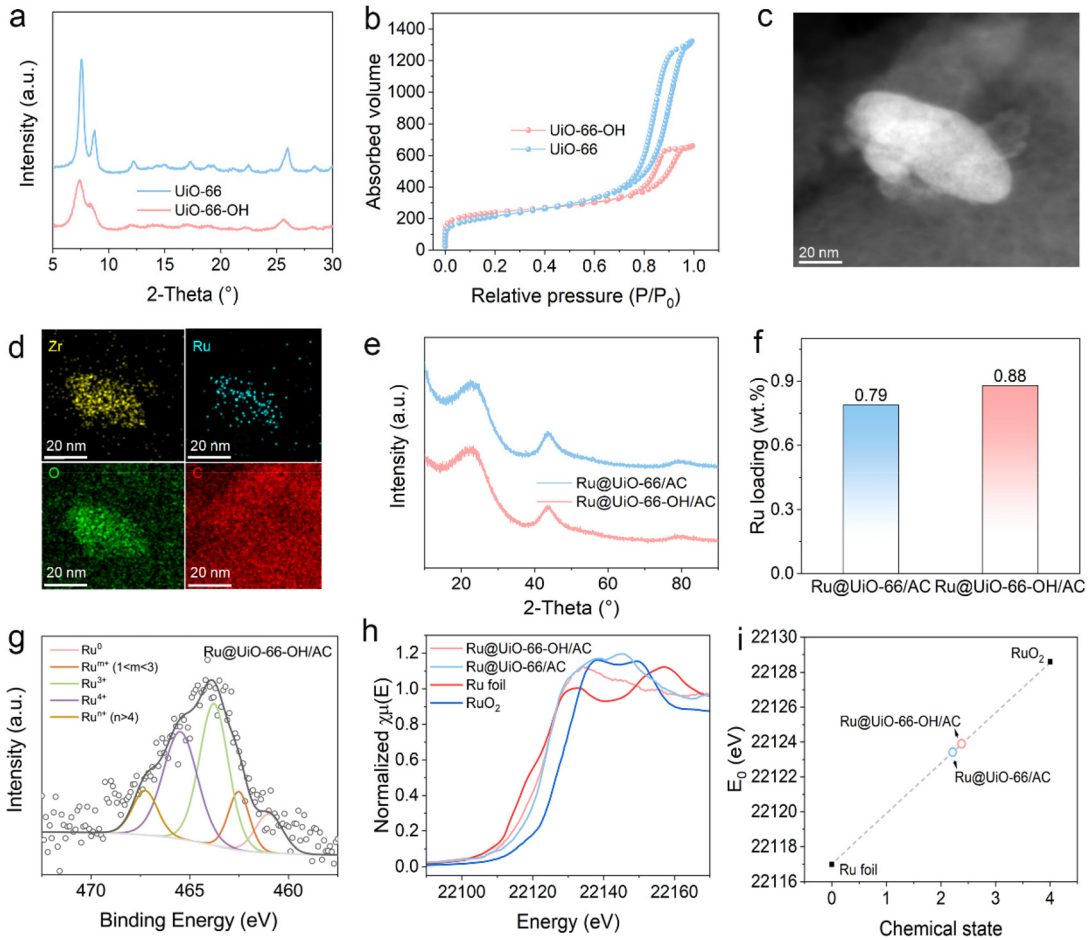

Fig. 1 Characterization of metal-organic frameworks: (a) XRD patterns and (b) FTIR spectra; (c) HADDF-TEM image and (d) relative elemental mapping images of the fresh Ru@UiO-66-OH/AC catalyst; (e) XRD patterns and (f) Ru content determined by ICP-OES of fresh Ru@UiO-66/AC and Ru@UiO-66-OH/AC; (g) Ru 3p XPS spectrum of Ru@UiO-66-OH/AC; (h) XANES spectra of Ru@UiO-66-OH/AC and Ru@UiO-66/AC; (i) edge energy of Ru catalysts.

channels of these two MOFs to decrease the agglomeration of active sites during the reaction, so the Ru precursor was mixed with the MOF first. To clarify the contribution of the channels from the MOF, the pore distributions of the pristine MOF and the relative Ru-based catalysts were analyzed (Fig. S1†). It was found that the contribution of the MOF in the Ru-based catalysts is mainly the micropores, whose sizes range from 1 to 2 nm. To further confirm the location of the Ru sites, the dispersion of Ru sites in the baseline catalyst was first analyzed through high-angle annular dark-field transmission electron microscopy (HAADF-TEM). As shown in Fig. S2,† there are obvious bright spots with an average size of 1.12 ± 0.31 nm, suggesting that the Ru sites easily aggregate during the preparation when activated carbon is used as the only support. However, when the MOF is introduced into the preparation of the catalyst, there is no obvious aggregation of Ru species (bright spots) at the region of activated carbon or at the boundary of the MOF (Fig. 1c and S3†). Taking Ru@UiO-66-OH/AC as an example, the elemental mappings of Zr and Ru (Fig. 1d) and the overlap image of the elemental mappings (Fig. S4†) were analyzed. It was found that the distribution of the Ru element is close to that of the Zr element, suggesting that the Ru sites are mainly encapsulated by the channels of the MOF. Based on the above analysis, we conclude that the Ru sites are encapsulated into the channels of the MOF. This high dispersion of Ru sites is also determined by XRD (Fig. 1e), where no metallic Ru species were detected in the Ru@UiO-66-OH/AC and Ru@UiO-66/AC samples. After analyzing the results of ICP-OES (Fig. 1f), both Ru-based catalysts with MOFs introduced have similar loadings. From the Ru 3p region (Fig. 1g, Fig. S5, S6 and Table S1†), we analyzed the chemical state of the Ru-based catalysts with MOFs introduced. The ratios of non-metallic Ru species (except Ru^0) in both Ru@UiO-66-OH/AC and Ru@UiO-66/AC are more than 85%. Furthermore, we employed XANES spectra to analyze the average oxidation state of Ru (Fig. 1h). After calculating the edge energy (E_0, Fig. 1i), it is illustrated that the average oxidation states of Ru in both Ru@UiO-66-OH/AC and Ru@UiO-66/AC are close, whose values are nearly 2.3. Both the results of XPS and XANES suggest that Ru sites mainly exist in a high valence state after

the MOF is introduced, which is consistent with the results from the XRD pattern.

3.2 Catalytic performances

The catalytic performances of the prepared catalysts in the acetylene hydrochlorination reaction were evaluated and compared in a fixed-bed reactor under the same conditions. As a reference, the AC-loaded Ru catalyst and the relative support were both compared under the same reaction conditions in this evaluation system. To investigate the catalytic role of the residual Zr element, we first evaluated UiO-66/AC, UiO-66-OH/AC and AC in control experiments for acetylene hydrochlorination. In the three experimental GHSVs (180 h^{-1}, 360 h^{-1} and 540 h^{-1}), the activities of the above three catalysts are similar and less than 25%, suggesting that the Zr sites play a weak role in acetylene hydrochlorination (Fig. 2a–c). However, when Ru sites are introduced into the support, both activities are significantly improved. Compared with the baseline catalyst, both Ru@UiO-66/AC and Ru@UiO-66-OH/AC show higher activity and stability, suggesting that the encapsulation of Ru sites plays a positive role in acetylene hydrochlorination. In particular, the Ru sites in the channel with –OH functional groups exhibit the highest conversion of 97.95%, suggesting that the microenvironment around the Ru sites is still a key factor in the reaction. Also, it is noted that the selectivity for VCM in both these supports and catalysts is close to 100% (Fig. S7†). With increasing GHSV (Fig. 2b and c), there is an obvious decrease in activity over the baseline catalyst while Ru@UiO-66-OH/AC still shows high and stable catalytic performance. For instance, the conversion of acetylene still remains 92.27% at a GHSV of 540 h^{-1}, which is over 40% higher than that of the baseline catalyst under the same conditions. In contrast, the stability of Ru@UiO-66/AC is poor under these high GHSV conditions. Furthermore, to investigate the dominant active sites of Ru species in Ru@UiO-66/AC and Ru@UiO-66-OH/AC, the relationship between the chemical state of Ru species and conversion is determined (Fig. S8†). It is found that the conversion obtained at a GHSV of 180 h^{-1} exhibits a linear relationship with the ratio of high-valent Ru species (Ru^{3+}, Ru^{4+} and Ru^{n+}), suggesting that high-valent Ru species in both Ru-based catalysts play a dominant role in this reaction.[16] Apart from the conversion of acetylene and selectivity for VCM, we also introduced a descriptor, that is deactivation rate,[37] to analyze the stability of the catalysts quantitatively. As shown in Fig. 2d, Ru@UiO-66-OH/AC always has a high stability, and the deactivation rates are both lower than 0.025% h^{-1} even when the GHSV is at a high level (540 h^{-1}). Based on these results, we demonstrate that the encapsulation

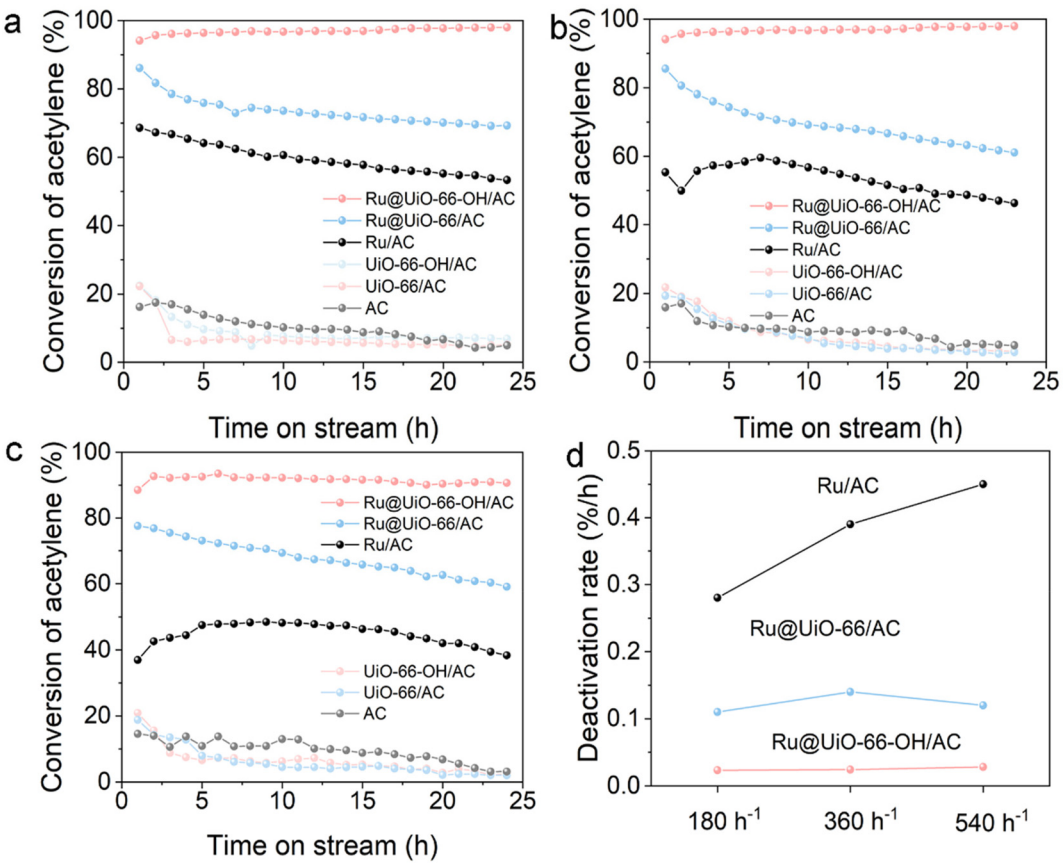

Fig. 2 Acetylene conversion with different catalysts at a GHSV of (a) 180 h^{-1}, (b) 360 h^{-1}, and (c) 540 h^{-1}; (d) deactivation rate for prepared catalysts. Reaction conditions: temperature = 180 °C and $V_{HCl}/V_{C_2H_2}$ = 1.15.

strategy for Ru sites and then the modification with –OH groups around the Ru sites both enhance the activity and stability in acetylene hydrochlorination.

3.3 Mechanism investigation

To clarify the role of UiO-66 in the Ru-based catalyst during the reaction, the properties of the used catalyst were investigated and analyzed. The dispersion of Ru sites in the used catalysts was performed by TEM. For the Ru@UiO-66-OH/AC catalyst, the structure of UiO-66-OH remains almost the same as that in the fresh catalyst (Fig. 3a). This indicates that the structure of UiO-66 remains stable during the reaction, agreeing well with the thermogravimetry/differential thermogravimetry (TG/DTG) curves of the fresh catalysts (Fig. S9†). As expected, the relative elemental mapping indicates that after the reaction, Ru species are still well dispersed with the Zr element, further suggesting that the Ru sites are encapsulated in the channels of the MOF (Fig. 3b). No obvious agglomeration of Ru sites illustrates the advantage of the encapsulation strategy. In contrast, the size of Ru sites in the baseline catalyst increases to 1.61 ± 0.43 nm after the reaction, demonstrating the agglomeration of Ru sites (Fig. S10†). The same results can also be obtained when the MOF is changed to UiO-66 (Fig. S11†). That is, the introduction of the MOF is beneficial for inhibiting the agglomeration of Ru species during the reaction due to the confinement provided by the unique pore structure. XRD patterns are analyzed to further confirm whether the active sites are aggregated in the catalysts (Fig. 3c and Fig. S12†). Compared with the fresh catalysts, the peak intensity of the used catalyst remained almost unchanged. There are only (002) and (101) peaks associated with the carbon carrier with no new characteristic peaks of metal Ru observed. Based on this stable dispersion of active sites, the deactivation rate decreases obviously.

Considering the extra channels introduced by the MOF, it is speculated that the coke deposition formed in the channels might affect the deactivation. To quantitatively determine the content of coke deposition, TG/DTG curves for fresh and used catalysts were employed (Fig. S13 and S14†). It is noted that all the values of coke deposition can be quantitatively calculated through the mass loss of the fresh and spent catalysts within the temperature range of 150–475 °C. We can see that before the addition of UiO-66 crystals, the coke deposition in the baseline catalyst Ru/AC is up to 8.4% (Fig. 3d). In contrast, the coke depositions of Ru@UiO-66/AC and Ru@UiO-66-OH/AC after the addition of UiO-66 are significantly reduced to 2.3%

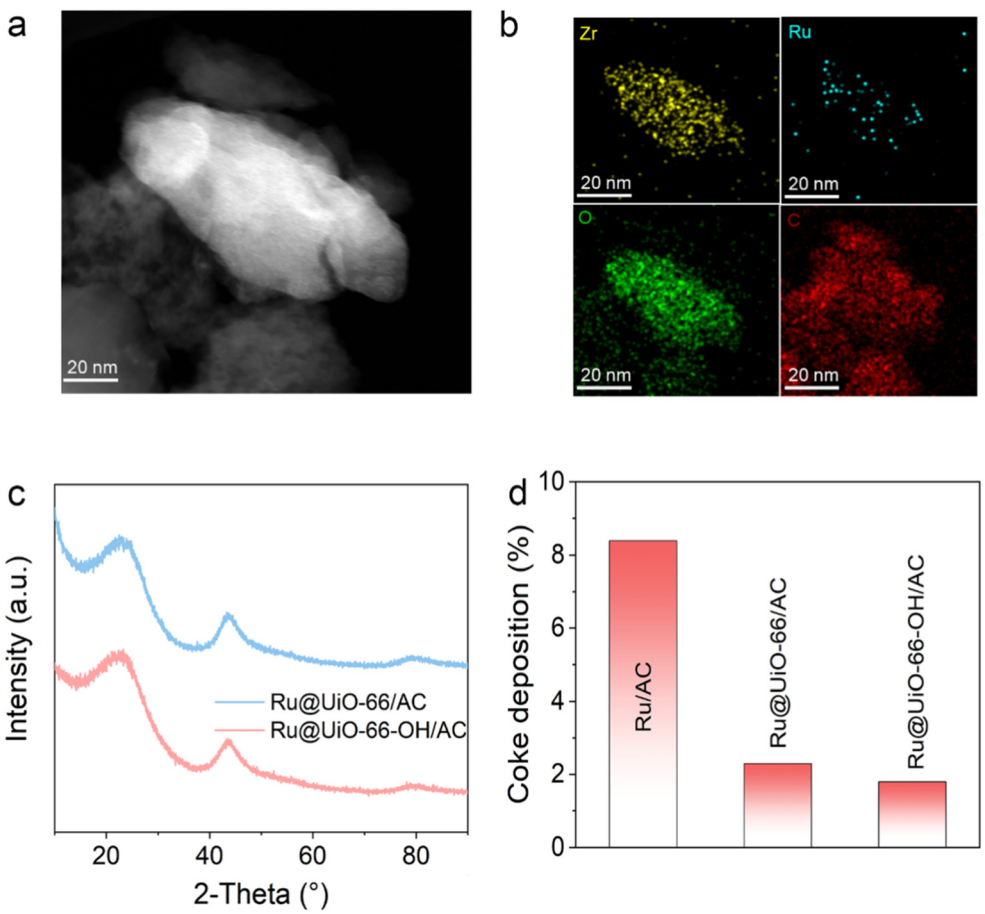

Fig. 3 (a) HADDF-TEM image and (b) relative elemental mapping of the used Ru@UiO-66-OH/AC catalyst; (c) XRD patterns of the used Ru@UiO-66/AC and Ru@UiO-66-OH/AC; (d) coke deposition analysis for the prepared catalysts.

and 1.8%, indicating that the addition of UiO-66 crystals has a significant inhibitory effect on coke deposition.

As we all know, the formation of coke results from acetylene. Also, the activity of the catalyst depends on the adsorption behavior of reactants. In this work, we introduce the MOF to create a stable dispersion of Ru sites as well as change the microenvironment around the Ru sites, enhancing the activity and stability of the Ru-based catalytic system. Therefore, it is speculated that in the Ru-based catalyst with the MOF introduced, the adsorption of reactants might change compared with the baseline catalyst. To reflect the adsorption and desorption behavior of the reactants involved, temperature-programmed desorption (TPD) with a reaction atmosphere was employed for both catalysts. Considering the pyrolysis of the MOF at high temperature, we first employed TPD under a helium atmosphere (He-TPD, Fig. S15†). In the He-TPD pro-

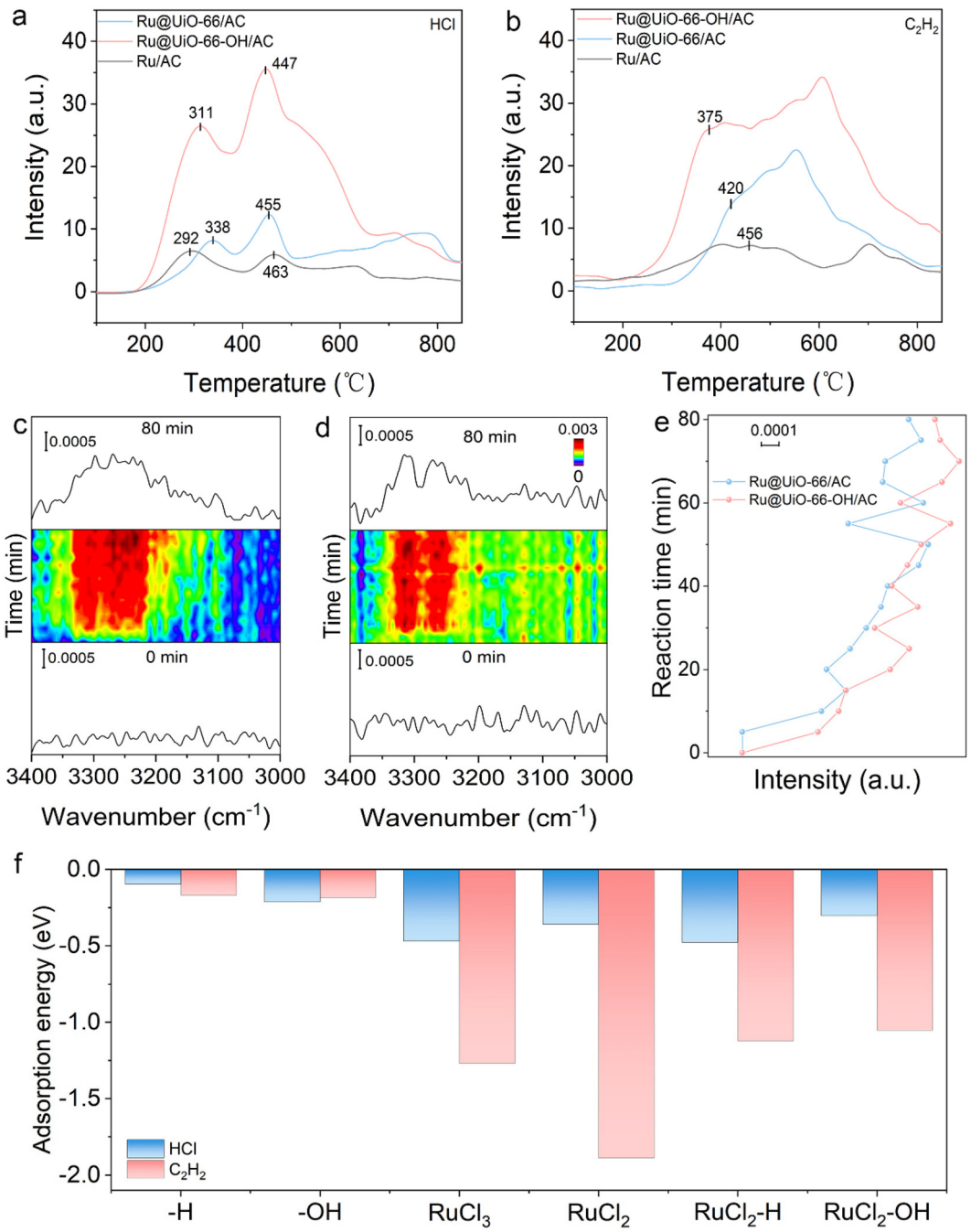

Fig. 4 (a) HCl-TPD and (b) C_2H_2-TPD profiles of Ru@UiO-66-OH/AC, Ru@UiO-66/AC and Ru/AC; *in situ* DRIFTS over (c) Ru@UiO-66-OH/AC and (d) Ru@UiO-66/AC; (e) intensity profiles of Ru@UiO-66-OH/AC and Ru@UiO-66/AC; (f) adsorption energies of C_2H_2 and HCl on the ligands in MOF and the relative Ru sites.

files, two obvious peaks appear around 400 and 600 °C, respectively, which arise from the pyrolysis of the MOF. Based on the results of He-TPD, we confirmed that Ru-based catalysts with MOFs introduced show a strong adsorption capacity for both reactants, compared with the baseline catalyst (Fig. 4a and b). The high concentration of HCl over local Ru sites is beneficial for enhancing the reaction rate. In particular, C_2H_2 molecules are more easily desorbed over Ru@UiO-66-OH/AC, inhibiting the rate of acetylene polymerization. The low rate of acetylene polymerization could decrease the coke deposition over Ru sites, agreeing with the results of coke deposition analysis (Fig. 3d). Also, the TPD under an NH_3 atmosphere (NH_3-TPD, Fig. S16†) for Ru@UiO-66/AC and Ru@UiO-66-OH/AC was employed to illustrate whether the MOF introduced affects the strong acidity of the Ru-based catalysts. Compared with Ru@UiO-66/AC, Ru@UiO-66-OH/AC has fewer strong-acidic sites, which is attributed to the peak around 381 °C.[38] This result suggests that the Ru sites encapsulated by UiO-66-OH are more stable during the reaction, agreeing well with the catalytic performance. The *in situ* diffuse reflectance infrared Fourier transform spectroscopy (*in situ* DRIFTS) over the surface of Ru@UiO-66-OH/AC and Ru@UiO-66/AC was conducted to verify the adsorption and diffusion of reactants. HCl and C_2H_2 were introduced into the reaction cell with a volume ratio of 1.15 and the spectra were obtained at 180 °C in an 80 min experiment. In the Ru@UiO-66-OH/AC and Ru@UiO-66/AC systems (Fig. 4c and d), these two characteristic peaks at around 3250 and 3310 cm^{-1} exist in the obtained spectra, which are both attributed to adsorbed acetylene molecules.[39] To quantitatively investigate the adsorption behavior and diffusion of reactants under reaction conditions, the intensity profile of the peak at 3250 cm^{-1} is shown in Fig. 4e. With the –OH group introduced into the channel, the acetylene molecules are more rapidly adsorbed onto the Ru sites, suggesting lower diffusion resistance of acetylene from the reaction bulk to the active sites. The results demonstrate that the modification of the microenvironment around Ru sites is beneficial for enhancing the activity of acetylene hydrochlorination.

In order to further investigate the effect of the introduction of the –OH group in the channel of UiO-66, we first selected two organic ligands including terephthalic acid (simplified as –H) and 2-hydroxyterephthalic acid (simplified as –OH). The –OH model has lower adsorption energy for HCl molecules, suggesting that the linker with hydroxyl groups in the MOF is able to provide more adsorption sites for HCl (Fig. 4f and S17†). Furthermore, considering the coordination environment around Ru as the primary factor for the catalyst's performance, two types of Ru species, namely $RuCl_2$ and $RuCl_3$, were selected and we then calculated the formation energies between the ligands and $RuCl_2$ and Ru species to determine the stable structure after coordination (Fig. S18†). Interestingly, both ligands coordinated with $RuCl_2$ (simplified as $RuCl_2$–H and $RuCl_2$–OH) have a lower formation energy compared with the structure coordinated with $RuCl_3$, suggesting a more favorable coordination structure. Therefore, we take the model coordinated with $RuCl_2$ as an example to determine the adsorption behavior of reactants over the coordinated Ru sites. As a reference, the uncoordinated Ru species ($RuCl_2$ and $RuCl_3$) are also investigated (Fig. S19†). Compared with $RuCl_2$ and $RuCl_3$, both the adsorption energies of C_2H_2 increase after coordination (Fig. 4f). In particular, with the existence of the –OH group, the Ru site exhibits the highest adsorption energy and increases to −1.05 eV. The higher adsorption energy illustrates that C_2H_2 molecules are easily desorbed from the active sites, agreeing well with the C_2H_2-TPD profiles. More importantly, if the C_2H_2 molecules do not over-occupy the active site, it is beneficial for decreasing the coke deposition, thus enhancing the stability of the catalyst. As for HCl, the adsorption energy still increases after the coordination of –OH groups, agreeing well with the lower desorption temperature in the TPD profiles.

The above results suggest that the linker with hydroxyl groups in the MOF is able to adsorb more hydrogen chloride and acetylene, agreeing well with the results from the TPD.

4. Conclusion

In conclusion, to inhibit the agglomeration of Ru sites in acetylene hydrochlorination, MOFs were introduced to encapsulate Ru sites. With the confinement effect of the channels in MOFs, the dispersion of Ru sites was uniform and stable before and after the reaction. Through evaluating the catalytic performance in acetylene hydrochlorination, both the activities of Ru-based catalysts with MOFs introduced were enhanced in contrast to the baseline catalyst. In order to decrease the diffusion resistance *via* changing the reaction microenvironment, we selected two types of MOFs, namely UiO-66 (with –H groups) and UiO-66-OH (with –OH groups). After characterization and DFT simulations, we demonstrated that more reactant molecules including HCl and C_2H_2 were adsorbed on Ru@UiO-66-OH/AC. Based on the positive effect of the UiO-66 metal framework, we achieved 92.27% conversion of acetylene and a 0.02% h^{-1} deactivation rate under a high GHSV(C_2H_2) of 540 h^{-1}. This work lays the groundwork for exploring Ru-based catalyst deactivation *via* skeleton materials with regular channels.

Author contributions

Digao Chai: conceptualization, data curation, formal analysis investigation, methodology, writing – review and editing. Qidi Liu: formal analysis, investigation, supervision, validation, visualization, writing – original draft, writing – review and editing. Yunsheng Dai: funding acquisition, resources, writing – review and editing. Yongsheng Xu: conceptualization, data curation, formal analysis, funding acquisition, methodology, resources, project administration, supervision, validation, visualization, writing – original draft, writing – review and editing. Yu Zi: investigation, writing – review and editing. Shuo Yang:

investigation, writing – review and editing. Yanzhao Dong: investigation, writing – review and editing. Dongyang Xie: investigation, writing – review and editing. Jinli Zhang: funding acquisition resources, project administration supervision, validation, visualization, writing – review and editing. Haiyang Zhang: conceptualization, data curation, formal analysis, funding acquisition, methodology, resources, software project administration, project administration, supervision, validation, visualization, writing – original draft, writing – review and editing.

Data availability

All data supporting the findings of this study are available within the paper and its ESI.†

Conflicts of interest

We declare that we do not have any commercial or associative interest that represents a conflict of interest in connection with the work submitted.

Acknowledgements

This work was supported by the National Natural Science Foundation of China (Grant No. 22068031), the Start-Up Foundation for Young Scientists of Shihezi University (No. RCZK202419), the Major Science and Technology Project of Yunnan Precious Metal Laboratory (YPML-2023050202), the Project of Achievement Transformation and Technology Extension of Shihezi University (CGZH202302), and the High-Level Talents Launching Program of Shihezi University (2022ZK002).

References

1 M. Y. Zhu, Q. Q. Wang, K. Chen, Y. Wang, C. F. Huang, H. Dai, F. Yu, L. H. Kang and B. Dai, *ACS Catal.*, 2015, **5**, 5306–5316.
2 B. L. Wang, Y. X. Yue, S. S. Wang, S. J. Shao, Z. Chen, X. H. Fang, X. X. Pang, Z. Y. Pan, J. Zhao and X. N. A. Li, *Green Energy Environ.*, 2021, **6**, 9–14.
3 Y. Liu, L. Zhao, Y. Zhang, L. Zhang and X. Zan, *Catalysts*, 2020, **10**, 1218–1228.
4 F. Feng, C. X. Jin, S. S. Wang, Y. X. Yue, D. Xu, K. X. Zhuge, P. Gao, J. Zhao, R. Q. Chang, L. L. Guo and H. Q. Dong, *Appl. Catal., A*, 2023, **661**, 119238–119263.
5 Z. Chen, Y. J. Chen, S. L. Chao, X. B. Dong, W. X. Chen, J. Luo, C. G. Liu, D. S. Wang, C. Chen, W. Li, J. Li and Y. D. Li, *ACS Catal.*, 2020, **10**, 1865–1870.
6 Y. Z. Dong, H. Y. Zhang, W. Li, M. X. Sun, C. L. Guo and J. L. Zhang, *J. Ind. Eng. Chem.*, 2016, **35**, 177–184.
7 J. H. Ke, Y. X. Zhao, Y. Yin, K. Chen, X. P. Duan, L. M. Ye and Y. Z. Yuan, *J. Rare Earths*, 2017, **35**, 1083–1091.
8 Y. X. Yue, B. L. Wang, J. L. Huang, S. S. Wang, C. X. Jin, R. Q. Chang, Z. Y. Pan, Y. H. Zhu, J. Zhao and X. N. Li, *ACS Appl. Mater. Interfaces*, 2024, **16**, 16106–16119.
9 J. Liu, G. J. Lan, Y. Y. Qiu, X. L. Wang and Y. Li, *Chin. J. Catal.*, 2018, **39**, 1664–1671.
10 B. Nkosi, N. J. Coville and G. J. Hutchings, *J. Chem. Soc., Chem. Commun.*, 1988, **1**, 71–72.
11 Y. Bao, X. Zheng, J. Cao, S. Li, Y. Tuo, X. Feng, M. Zhu, B. Dai, C. Yang and D. Chen, *Nano Res.*, 2022, **16**, 6178–6186.
12 M. Cai, H. Zhang, B. Man, J. Li, L. Li, Y. Li, D. Xie, R. Deng and J. Zhang, *Catal. Sci. Technol.*, 2020, **10**, 3552–3560.
13 Z. Guo, W. Peng, J. Li, F. Li, Q. Zhang, L. Yang, D. Xie, Y. Dong, J. Zhang and H. Zhang, *New J. Chem.*, 2023, **47**, 14019–14029.
14 S. K. Kaiser, R. Lin, F. Krumeich, O. V. Safonova and J. Pérez-Ramírez, *Angew. Chem., Int. Ed.*, 2019, **58**, 12297–12304.
15 H. Li, B. Wu, J. Wang, F. Wang, X. Zhang, G. Wang and H. Li, *Chin. J. Catal.*, 2018, **39**, 1770–1781.
16 J. Li, H. Zhang, M. Cai, L. Li, Y. Li, R. Zhao and J. Zhang, *Appl. Catal., A*, 2020, **592**, 117431–117441.
17 J. Li, H. Zhang, H. Liang, L. Li and J. Zhang, *Mol. Catal.*, 2022, **519**, 112142–112152.
18 Y. Li, F. Wang, B. Wu, X. Wang, M. Sun, Z. Zhang and X. Zhang, *Catal. Sci. Technol.*, 2022, **12**, 5086–5096.
19 X. Tao, F. Chen, Y. Xie, X. Cheng, X. Liu and G. Gao, *J. Taiwan Inst. Chem. Eng.*, 2021, **126**, 80–87.
20 S. Wang, L. Wan, C. Jin, T. Wang, K. Zhuge, Y. Yue, H. Cai, B. Wang, R. Chang, J. Zhao and X. Li, *Appl. Catal., A*, 2023, **665**, 119382–119413.
21 X. Wang, G. Lan, Z. Cheng, W. Han, H. Tang, H. Liu and Y. Li, *Chin. J. Catal.*, 2020, **41**, 1683–1691.
22 M. Zhang, H. Zhang, F. Li, W. Peng, L. Yao, Y. Dong, D. Xie, Z. Liu, C. Li and J. Zhang, *ACS Sustainable Chem. Eng.*, 2022, **10**, 13991–14000.
23 M. Zhang, H. Zhang, F. Li, L. Yao, W. Peng and J. Zhang, *Catal. Sci. Technol.*, 2022, **12**, 4255–4265.
24 Y. Fan, Z. Liu, S. Sun, W. Huang, L. Ma, Z. Qu, N. Yan and H. Xu, *ACS Appl. Mater. Interfaces*, 2023, **15**, 24701–24712.
25 Y. Jia, Y. Nian, J. Zhang and Y. Han, *Mol. Catal.*, 2021, **513**, 111826–111835.
26 J. Li, H. Zhang, H. Liang, L. Yao, C. Li and J. Zhang, *Mol. Catal.*, 2023, **543**, 113158–113168.
27 H. Zhang, T. Zhang, Y. Jia, J. Zhang and Y. Han, *J. Phys. Chem. Lett.*, 2021, **12**, 7350–7356.
28 L. Hou, J. Zhang, Y. Pu and W. Li, *RSC Adv.*, 2016, **6**, 18026–18032.
29 J. Q. Dong, X. Han, Y. Liu, H. Y. Li and Y. Cui, *Angew. Chem., Int. Ed.*, 2020, **59**, 13722–13733.
30 S. Dissegna, K. Epp, W. R. Heinz, G. Kieslich and R. A. Fischer, *Adv. Mater.*, 2018, **30**, 3–23.
31 S. Won, S. Jeong, D. Kim, J. Seong, J. Lim, D. Moon, S. B. Baek and M. S. Lah, *Chem. Mater.*, 2022, **34**, 273–278.
32 L. Feng, J. D. Pang, P. She, J. L. Li, J. S. Qin, D. Y. Du and H. C. Zhou, *Adv. Mater.*, 2020, **32**, 1–23.

33 W. Xu, M. Dong, L. Di and X. Zhang, *Nanomaterials*, 2019, **9**, 1432–1434.
34 L. D. Hao, X. Y. Li, M. J. Hurlock, X. M. Tu and Q. Zhang, *Chem. Commun.*, 2018, **54**, 11817–11820.
35 J. P. Perdew, K. Burke and M. Ernzerhof, *Phys. Rev. Lett.*, 1996, **77**, 3865–3868.
36 F. Joly, P. Devaux, T. Loiseau, M. Arab, B. Morel and C. Volkringer, *Microporous Mesoporous Mater.*, 2019, **288**, 109564.
37 S. K. Kaiser, R. H. Lin, F. Krumeich, O. V. Safonova and J. Pérez-Ramírez, *Angew. Chem., Int. Ed.*, 2019, **58**, 12297–12304.
38 O. M. AlAmoudi, W. Ullah Khan, D. Hantoko, I. A. Bakare, S. A. Ali and M. M. Hossain, *Fuel*, 2024, **372**, 132230–132244.
39 Y. R. Fan, H. M. Xu, G. Q. Gao, M. M. Wang, W. J. Huang, L. Ma, Y. C. Yao, Z. Qu, P. F. Xie, B. Dai and N. Q. Yan, *Nat. Commun.*, 2024, **15**, 6035.